



# Determination of Acetylcholinesterase Activity Based on Ratiometric Fluorescence Signal Sensing

Fengju Zhao<sup>1</sup> · Hui Guo<sup>1,2,3</sup> · Wei Yang<sup>1</sup> · Lili Guo<sup>1</sup> · Jiaxin Li<sup>1</sup> · Hanqi Chen<sup>1</sup>

Received: 29 February 2024 / Accepted: 5 April 2024

© The Author(s), under exclusive licence to Springer Science+Business Media, LLC, part of Springer Nature 2024

## Abstract

Acetylcholinesterase (AChE) plays an important role in the treatment of human diseases, environmental security and global food supply. In this study, the simple fluorescent indicators and MnO<sub>2</sub> nanosheets were developed and integrated to establish a ratiometric fluorescence sensing system for the detection of AChE activity. Two fluorescence signals could be recorded independently at the same excitation wavelength, which extended the detection range and enhanced the visibility of results. Fluorescence of F-PDA was quenched by MnO<sub>2</sub> nanosheets on account of inner filtering effect. Meanwhile, the nonfluorescent OPD was catalytically oxidized to 2,3-diaminophenazine by MnO<sub>2</sub> nanosheets. The acetylcholine (ACh) was catalytically hydrolyzed by AChE to enzymatic thiocholine, which decomposed MnO<sub>2</sub> to Mn<sup>2+</sup>, recovered the fluorescence of F-PDA and reduced the emission of ox-OPD. Utilizing the fluorescence intensity ratio  $F_{468}/F_{558}$  as the signal readout, the ratiometric fluorescence method was established to detect AChE activity. Under the excitation wavelength of 410 nm, the ratio  $F_{460}/F_{558}$  against the AChE concentration demonstrated two linear relationships in the range 0.05–1.0 and 1.0–50 U·L<sup>-1</sup> with a limit of detection (LOD) of 0.073 U·L<sup>-1</sup>. The method was applied to the detection of AChE activity and the analysis of the inhibitor Huperzine-A. Due to the advantages of high sensitivity and favorable selectivity, the method possesses an application prospect in the activity detection of AChE and the screening of inhibitors.

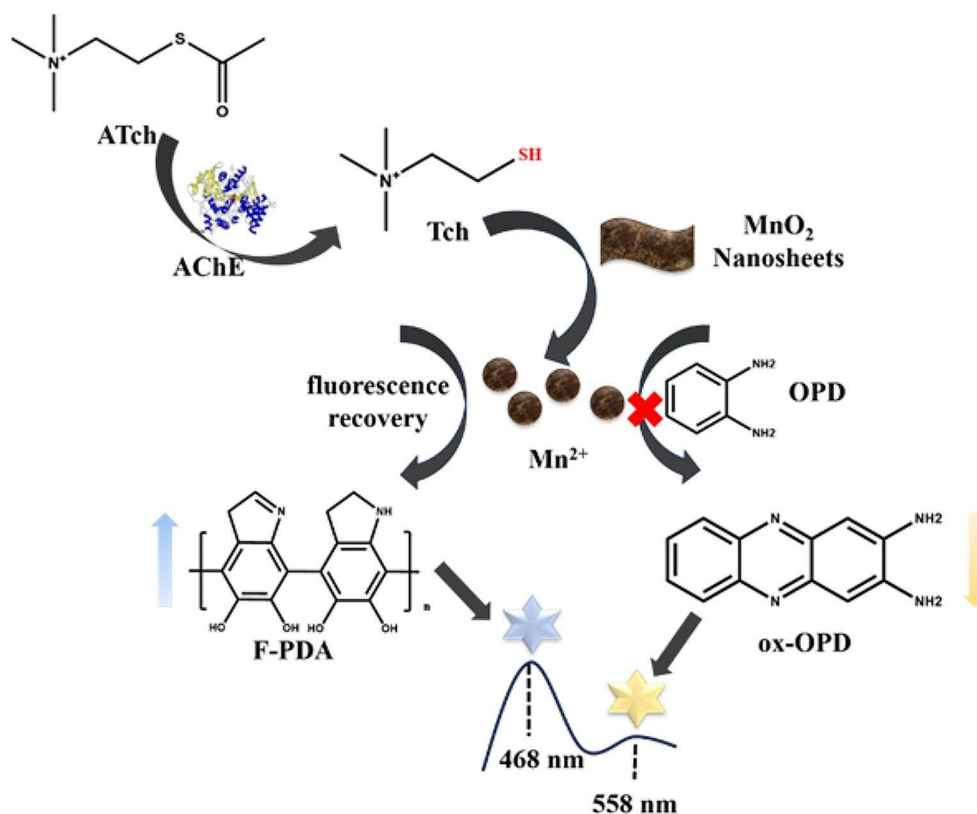
✉ Hui Guo  
tggh635@163.com

<sup>1</sup> College of Pharmaceutical Science, Zhejiang University of Technology, Hangzhou, Zhejiang Province 310014, P.R. China

<sup>2</sup> Key Laboratory for Green Pharmaceutical Technologies and Related Equipment of Ministry of Education, Zhejiang University of Technology, Hangzhou, Zhejiang Province 310014, P.R. China

<sup>3</sup> Key Laboratory of Pharmaceutical Engineering of Zhejiang Province, Zhejiang University of Technology, Hangzhou, Zhejiang Province 310014, P.R. China

## Graphical Abstract



**Keywords** MnO<sub>2</sub> nanosheets · Ratiometric fluorescence · Acetylcholinesterase · o-Phenylenediamine · Fluorescent polydopamine nanoparticle · Inhibitor screening

## Introduction

Acetylcholinesterase (AChE) as a primary cholinesterase in nervous system functioning is responsible for biological signal transmission [1]. It can hydrolyze the neurotransmitter acetylcholine (ATCh) into choline and acetic acid, playing an important role in memory and learning [2]. Neurobiological studies have shown that fluctuations in AChE levels are associated with various diseases, for example diabetes, Parkinson's and Alzheimer's [3]. AChE has become an important biomarker and drug target in clinical diagnosis and detoxification therapy [4]. Among them, Alzheimer's disease is one of the most common major causes of Alzheimer's disease, which is accompanied by memory dysfunction, behavioral disorders, and cognitive impairment [5]. So far, most AChE inhibitors, tacrine, neostigmine and huperzine-A can inhibit the activity of AChE to increase the level of ATCh, and thus become effective drugs for treating these diseases [6]. However, these drugs are clinically associated with gastrointestinal side effects. On the other hand, a large excess of inhibitors has an irreversible inhibitory effect on

AChE activity, which eventually leads to neurotransmission and metabolic disorders and damages the human cholinergic system [7]. Therefore, accurate and effective detection of acetylcholinesterase activity and its inhibitors are important for human health, early clinical diagnosis and treatment of the disease.

To date, various strategies have been explored to monitor AChE activity, such as the colorimetric [8], fluorometric [2], chemiluminescent [9], and electrochemical methods [10]. Commonly used colorimetric methods often encounter problems such as low sensitivity, false positive effects, and are prone to interference, which reduces the reliability of the results [2]. Electrochemical analysis has higher sensitivity, but electrode contamination and the necessity of specialized equipment limit its application [11]. The fluorescent method has been widely used in the detection of AChE because of high sensitivity, rapidity, low cost, and easy operation [12]. A label-free single-particle enumeration method was developed by Han's group for the quantitative detection of AChE activity and this method is based on the fluorescence resonance energy transfer (FRET) that occurs between fluorescent conjugated polymer nanoparticles and

MnO<sub>2</sub> nanosheets [13]. However, the application of some commonly used fluorescence methods, such as organic dyes and semiconductor quantum dots, is limited due to their high toxicity and poor biocompatibility [14]. Other methods based on fluorescent nanomaterials also have some disadvantages, such as more operation steps, complex probe preparation process and long reaction time [14]. Therefore, it is important to develop a simple, inexpensive and highly sensitive assay for AChE activity.

MnO<sub>2</sub> nanosheets have attracted widespread attention because of its large specific surface area, excellent biocompatibility, redox property, wide absorption band (300–600 nm), peroxidase-like activity, etc. Halawa's group achieved the self-assembly of acridine fluorophore lucigenin on MnO<sub>2</sub> nanosheets by electrostatic interactions, enabling ultrasensitized detection of glutathione [15]. When it comes to the use of MnO<sub>2</sub> nanosheets for modulating fluorescent signals, most systems rely on the quenching effect of these nanosheets on fluorescent substances. However, not much research has been done to explore the role of MnO<sub>2</sub> nanosheets in generating fluorescence. Fan's group for the first time expanded the application of oxidase-like property of MnO<sub>2</sub> nanosheet to fluorescent substrates of peroxidase [16]. However, the present fluorescence sensing system utilizing MnO<sub>2</sub> nanosheets for AChE activity detection is associated with several limitations. Throughout the entire detection process, the intensity of single channel fluorescence is susceptible to interference from factors unrelated to AChE. In addition, the visibility level is inadequate, while the range of detection is limited [17]. To tackle this issue, ratiometric fluorescence has been suggested as a solution, which can alleviate the problem of selectivity in fluorescence analysis and sensing techniques. This has the potential to enhance the utility of fluorescence analysis techniques in everyday life and industrial processes [18].

The construction of optical ratiometric sensing systems with excellent performance is still worthy of attention and exploration in recent years. In this study, a biosensing technique with low cost, fast response, high sensitivity, and easy operation was developed by combining the excellent performance of MnO<sub>2</sub> nanosheets with the simple fluorescent indicator. In this work, the detection principle is based on utilizing AChE to indirectly change MnO<sub>2</sub> nanosheets' physicochemical features, resulting in multichannel ratiometric fluorescence signal changes, which permits detecting AChE activity.

## Materials & Methods

### Materials and Reagents

Triple-distilled water was used throughout the experimental process. The analytical chemicals including ATCh, glucose(Glu), L-Serine(Ser), and Amylase(Amy) were obtained from Shanghai Macklin Biochemical Co., Ltd. (Shanghai, China). Acetylcholinesterase (AChE),  $\beta$ -Glucosidase, Dopamine hydrochloride(PDA), and bovine serum albumin (BSA) was purchased from Shanghai yuanye Bio-Technology Co., Ltd. (Shanghai, China). Cellulase, lipase, huperzine-A, tetramethylammonium hydroxide solution (TMA·OH, 25 wt%), MnCl<sub>2</sub>·4H<sub>2</sub>O, and o-Phenylenediamine(OPD) were purchased from Aladdin Ltd. (Shanghai, China). Hydrogen peroxide (H<sub>2</sub>O<sub>2</sub>, 30 wt%), sodium dihydrogen phosphate, and disodium hydrogen phosphate were purchased from Sinopharm Chemical Reagent Co., Ltd (Shanghai, China). All reagents were of analytical grade and without any further purification.

### Preparation of MnO<sub>2</sub> Nanosheets

MnO<sub>2</sub> nanosheets were prepared according to the previously reported method with minor modifications [19]. Water-soluble MnO<sub>2</sub> nanosheets were prepared as follows: 4.375 mL of tetramethylammonium hydroxide solution (25 wt%) and 2.0 mL of H<sub>2</sub>O<sub>2</sub> (30 wt%) were mixed and then the mixture was diluted to 20 mL with ultrapure water. The solution was quickly mixed with 10 mL of MnCl<sub>2</sub>·4H<sub>2</sub>O (0.3 M), causing it to immediately turn brown-black. The solution was shaken for 12 h in a water bath shaker at room temperature, the suspension formed. Next, the precipitate were collected from the suspension by centrifugation at 12,000 rpm for 10 min, followed by washing three times with ethanol and water. Finally, MnO<sub>2</sub> nanosheets obtained by centrifugation was freeze-dried under vacuum for 12 h. Next, 0.01 g of MnO<sub>2</sub> nanosheets were dispersed in 100 mL water by ultrasonic cell crusher for 15 min (200 W, 5 s ultrasound, 2 s interval) and stored at 4 °C for further use.

### Synthesis of F-PDA Nanoparticles

F-PDA nanoparticles were synthesized according to the previously reported methods with a minor modification [20]. First, 1 mL of dopamine hydrochloride solution (20 mM) and 800  $\mu$ L of sodium hydroxide solution (100 mM) were mixed with 20 mL phosphate buffer solution (PB, pH = 7.4, 2 mM). After being stirred at room temperature for 1 h, the solution underwent from colorless to brown. At this point, 1 mL of hydrochloric acid solution (0.2 M) was added to the mixture, resulting in a rapid decrease in polymerization

rate. Then, after magnetic stirring for 0.5 h, a bright brown solution was obtained and stored at room temperature away from light.

### Assays for AChE Activity

Various concentrations of AChE were mixed with 200  $\mu\text{L}$  of ATCh (700  $\mu\text{M}$ ) for 30 min at 37  $^{\circ}\text{C}$ . Then, 200  $\mu\text{L}$  of  $\text{MnO}_2$  (30  $\mu\text{g}\cdot\text{mL}^{-1}$ ) were added to the above mixture. After reacting, 100  $\mu\text{L}$  of F-PDA and 200  $\mu\text{L}$  of OPD (4.2  $\text{mg}\cdot\text{mL}^{-1}$ ) was introduced into the solution and remained the reaction for 60 min at 37  $^{\circ}\text{C}$ . Dilute the mixture to 1mL with PB buffer (pH=7, 2 mM). The fluorescence intensities were measured at 468 and 558 nm with an excitation wavelength of 410 nm, using a 5 nm slit width for both excitation and emission. A calibration curve was constructed for the detection of AChE by plotting the fluorescence intensity ratio  $F_{468}/F_{558}$  at 468 and 558 nm on the y-axis and the concentration of AChE on the x-axis.

### Screening of Inhibitor

In order to verify the feasibility of this method for inhibitor screening, 200  $\mu\text{L}$  of huperzine-A with different concentrations and 200  $\mu\text{L}$  of 30  $\text{U}\cdot\text{L}^{-1}$  AChE were mixed and incubated at 37  $^{\circ}\text{C}$  for 10 min. Then, 200  $\mu\text{L}$  of 700  $\mu\text{M}$  ATCh was added and incubated at 37  $^{\circ}\text{C}$  for 30 min. Subsequently, 100  $\mu\text{L}$  of F-PDA and 50  $\mu\text{L}$  of  $\text{MnO}_2$  were added, and the reaction continued for 10 min. Finally, 200  $\mu\text{L}$  of

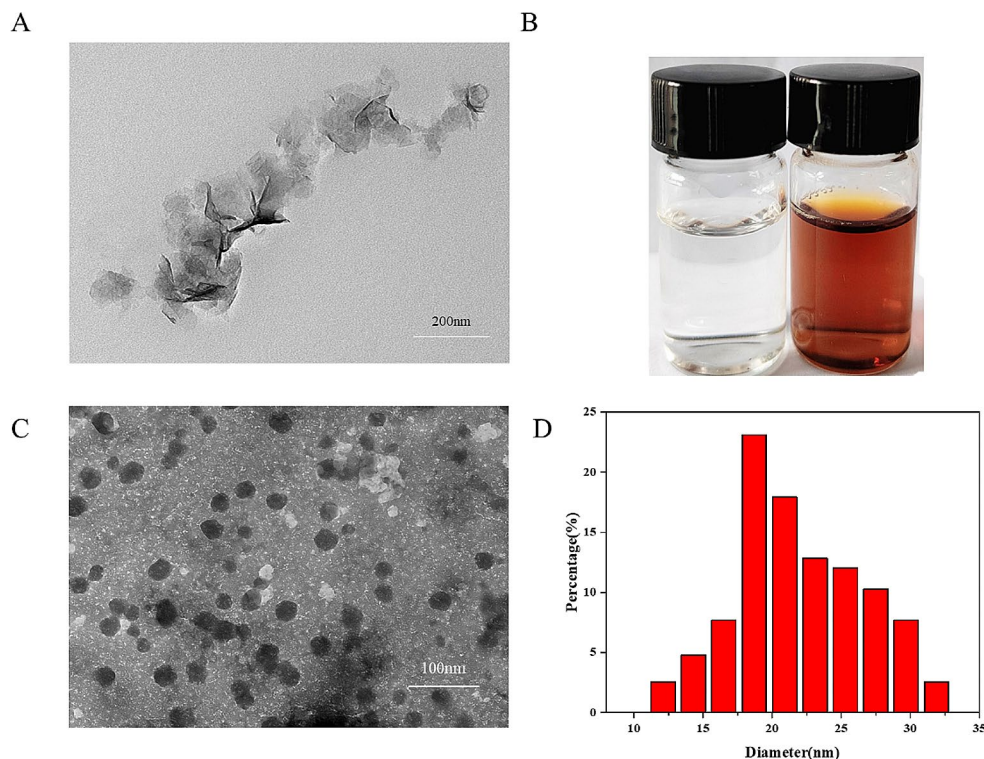
OPD (4.2  $\text{mg}\cdot\text{mL}^{-1}$ ) was added and incubated at 37  $^{\circ}\text{C}$  for 60 min. Dilute the mixture to 1 mL with PB buffer (pH=7.4, 2 mM). After that, the fluorescence intensity was measured according to the same measurement conditions for AChE detection.

## Results and Discussion

### Preparation and Characterization of $\text{MnO}_2$ Nanosheets and F-PDA Nanoparticles

As shown in Fig. 1A,  $\text{MnO}_2$  nanosheets have a two-dimensional sheet structure and this special nanostructure provides a large surface area for the  $\text{MnO}_2$  nanosheets [21]. As shown in Fig. 1B, the color of the solution changed from transparent to dark brown after the reaction, indicating the formation of  $\text{MnO}_2$  nanosheets. The nanosheets were characterised by UV-vis spectroscopy and FT-IR, Fig. S1 demonstrates that  $\text{MnO}_2$  nanosheets have a broad absorption peak within the 300–600 nm range with a maximum at 375 nm due to the d–d transition in the ligand field of  $\text{MnO}_2$  octahedra [22]. The FT-IR absorption peak of as-prepared  $\text{MnO}_2$  nanosheets located at 479  $\text{cm}^{-1}$  was attributed to the stretching vibration modes of Mn–O bond (Fig.S2), fully indicating the formation of  $\text{MnO}_2$  nanosheets [23]. The microstructure and morphology of the F-PDA nanoparticles were confirmed by TEM images. As shown in Fig. 1C and D, the synthesized F-PDA is spherical and the particle size is about 11 ~ 33 nm.

**Fig. 1** (A) TEM images of  $\text{MnO}_2$  nanosheets. (B) Images of  $\text{MnCl}_2$  solution (left) and  $\text{MnO}_2$  nanosheets solution (right). (C) TEM image of F-PDA in their dispersed state. (D) Size distribution of F-PDA nanoparticles in diameter measured by TEM.



As presented in Fig. S3, the F-PDA have a characteristic absorption peak at around 287 nm in its UV-Vis absorption spectra. As further illustrated in FT-IR spectrum of F-PDA, the absorptions at  $3423\text{ cm}^{-1}$  is attributed to the stretching vibration of -OH group. The absorption peak at  $1629\text{ cm}^{-1}$  is the C=C stretching vibration, and the absorption peak at  $1401\text{ cm}^{-1}$  is the bending vibration of N-H on the aromatic ring (Fig. S4). It is evident that fluorescent nanoparticles of F-PDA have been successfully synthesised. In addition, the fluorescence quantum yield of F-PDA was calculated using the reference method, using quinine sulfate as the reference solution, the results are shown in the Table S1. According to the equation, the fluorescence quantum yield was 10.9%.

### Feasibility and Mechanism of Detection

The feasibility of  $\text{MnO}_2$ -F-PDA-OPD system for qualitative detection of AChE was first assessed as shown in Fig. 2. Firstly,  $\text{MnO}_2$  nanosheets can quench the fluorescence of F-PDA in the two-channel ratio fluorescence mode. F-PDA has many functional groups, including planar indolyl, orthoquinyl, carboxyl, amino, imine, and phenol groups, which can specifically explain the strong adhesion ability of F-PDA [24]. Based on the inherent adhesion of F-PDA, F-PDA nanoparticles are easily adsorbed on the surface of  $\text{MnO}_2$  nanosheets to form F-PDA- $\text{MnO}_2$  nanocomposites through non-covalent binding interactions. In addition,  $\text{MnO}_2$  nanosheets could oxidise non-fluorescent O-phenendiamine to ox-OPD with yellow fluorescence ( $\lambda_{\text{em}}=558\text{ nm}$ ), because  $\text{MnO}_2$  nanosheets used their oxidase-like activity to catalyse the oxidation of non-fluorescent OPD to form 2, 3-diaminophenolazine with yellow fluorescence [25]. Thus, in the initial state, the constructed  $\text{MnO}_2$ -F-PDA-OPD sensing system exhibits strong ox-OPD fluorescence emission ( $\lambda_{\text{em}}=558\text{ nm}$ , channel 1) and weak F-PDA fluorescence emission ( $\lambda_{\text{em}}=468\text{ nm}$ , channel 2) under a single 410 nm excitation light excitation (Fig. 2A, green lines). As depicted in Fig. 2B, there was a relatively large overlap region between the broad absorption spectrum in the range of 300–600 nm of  $\text{MnO}_2$  nanosheets and the fluorescence emission and excitation spectrum of F-PDA nanoparticles. In addition, as shown in Fig. 2C, the characteristic absorption peaks of F-PDA and  $\text{MnO}_2$  nanosheets are 285 and 380 nm, respectively. After mixing F-PDA and  $\text{MnO}_2$  nanosheets, no new peak appears, indicating that no complex is formed between F-PDA and  $\text{MnO}_2$ . Therefore, the quenching mechanism of F-PDA nanoparticles by  $\text{MnO}_2$  nanosheets was considered to stem from IFE [26].

In addition, the feasibility of the method was verified by the UV-vis absorption spectra of Fig. 2D. When AChE and ATCh coexisted, the absorbance of  $\text{MnO}_2$  nanosheets at 380 nm decreased, which also indicated that the  $\text{MnO}_2$

nanosheets were partially decomposed. Unlike  $\text{MnO}_2$  nanosheets, the  $\text{Mn}^{2+}$  generated by degradation do not have specific light absorbing ability and oxidase-like activity, which changes the fluorescence intensity of the ratiometric fluorescence sensing system. As a result, the degree of fluorescence quenching of F-PDA by  $\text{MnO}_2$  nanosheets was weakened, as evidenced by the fluorescence recovery of F-PDA, and the degree of oxidation of OPD was reduced, as evidenced by the weakening of the fluorescence intensity of ox-OPD (Fig. 2A, green and purple lines). The two-channel emission intensity ratio  $F_{468}/F_{558}$  increased. The content of  $\text{MnO}_2$  nanosheets is AChE activity dependent, while the fluorescence recovery degree of F-PDA and the fluorescence intensity of ox-OPD are  $\text{MnO}_2$  nanosheets content dependent. Therefore, the two-channel intensity ratio  $F_{468}/F_{558}$  of the ratiometric fluorescence sensing system  $\text{MnO}_2$ -F-PDA-OPD will have a certain stoichiometric relationship with AChE activity, which can realise the quantitative fluorescence detection of AChE activity. At the same time, a good visualisation of the AChE activity detection results can be achieved by observing the fluorescence colour changes induced by changes in the sensing system  $F_{468}/F_{558}$ . This is the principle of the two-channel ratiometric fluorescence sensing system for the detection of AChE activity based on the light-absorbing capacity of  $\text{MnO}_2$  nanosheets and the activity of oxidase-like enzymes in this study.

### Optimization of Experimental Conditions

Firstly, it is necessary to select the excitation wavelength. Since the ratiometric fluorescence detection system contains more than one fluorescence detection signal, it is necessary to select the appropriate excitation wavelength for two fluorescence detection signals by considering the excitation wavelengths of the two fluorescence detection signals. In this study, F-PDA and OPD were used as fluorescence signal conversion units to provide blue channel ( $\lambda_{\text{em}}=468\text{ nm}$ ) and yellow channel ( $\lambda_{\text{em}}=558\text{ nm}$ ) fluorescence signals, respectively. In the constructed sensor system, the fluorescence spectra of F-PDA and OPD are shown in Fig. S5, and it can be seen that the maximum excitation wavelengths of both F-PDA and OPD are around 410 nm. Therefore, 410 nm was chosen as the wavelength of the incident excitation light. Under 410 nm excitation light, the fluorescence emission intensity of the F-PDA solution gradually increased with increasing F-PDA content (Fig. 3A). To attain enough fluorescence emission intensity and visualize detection outcomes, 100  $\mu\text{L}$  of F-PDA was chosen for constructing the sensing system. The F-PDA nanoparticles served as the blue channel fluorescence signal conversion unit in the ratiometric fluorescence mode. The blue fluorescent F-PDA nanoparticles showed a quenching reaction



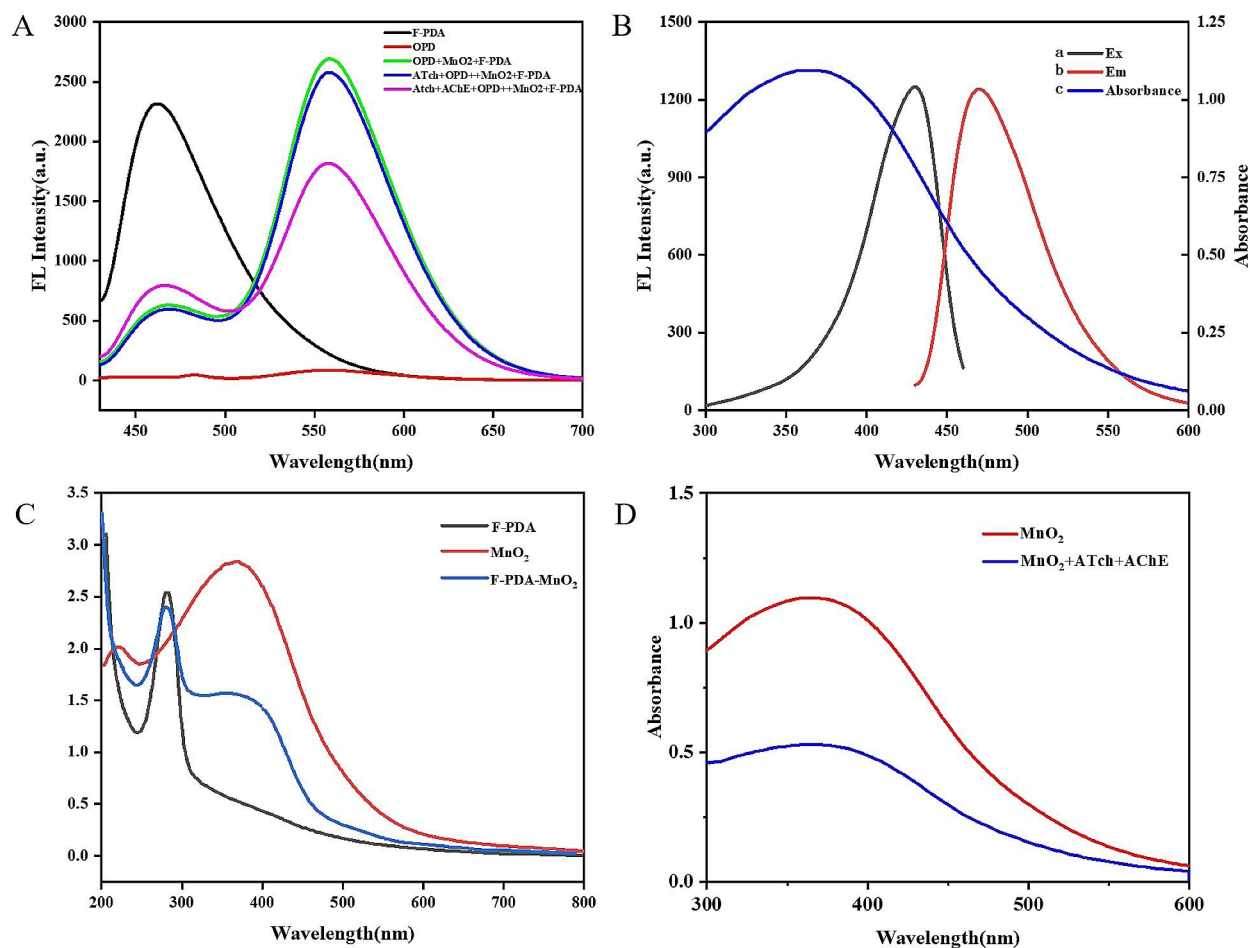


**Fig. 2** (A) Fluorescence emission spectra of different solutions. (B) Overlay of the excitation (a) and emission (b) spectra of F-PDA and the UV-vis absorption spectrum (c) of MnO<sub>2</sub> nanosheets.

time of 4 min (Fig. S6). Based on this, a negative correlation between the concentration of MnO<sub>2</sub> nanosheets and the fluorescence intensity of the synthesised F-PDA nanoparticles was observed (Fig. 3B). It was found that an inadequate number of MnO<sub>2</sub> nanosheets had a low degree of fluorescence quenching of F-PDA nanoparticles. On the other hand, an excessive number of MnO<sub>2</sub> nanosheets were found to be unfavourable for the detection of low-activity AChE. As a result, 30  $\mu\text{g}\cdot\text{mL}^{-1}$  was chosen to be the optimal concentration of MnO<sub>2</sub> nanosheets. In addition, the effect of OPD content on the fluorescence intensity of the ratiometric fluorescence system was also investigated. Figure 3C illustrate the optimisation of OPD concentration. The ratio  $F_{468}/F_{558}$  gradually decreased and stabilised with increasing OPD concentration. The optimum reaction concentration of OPD was determined to be 4.2  $\text{mg}\cdot\text{mL}^{-1}$ .

In addition, the absorbance of MnO<sub>2</sub> nanosheets was measured after reacting with a mixture of Tch generated by

(C) UV-vis absorption spectra of F-PDA, MnO<sub>2</sub> nanosheets, and F-PDA-MnO<sub>2</sub> (D) UV-vis absorption spectra of MnO<sub>2</sub> nanosheets and MnO<sub>2</sub>-ATCh-AChE.

the reaction of ATCh and AChE for different times. As can be seen in Fig. S7, the TCh-induced absorbance of MnO<sub>2</sub> nanosheets decreased rapidly within 1 min and levelled off after 4 min. As presented in Fig. 3D, when the concentration of ATCh was low (100  $\mu\text{M}$ ), even with the use of highly active AChE to catalyze the ATCh reaction, a sufficient amount of TCh could not be produced to reduce manganese dioxide (MnO<sub>2</sub>) to manganese ion (Mn<sup>2+</sup>), and as a result, the change in the intensity ratio of two channels  $F_{468}/F_{558}$  was not significant. As the concentration of ATCh and AChE activity gradually increased, the enzymatic reaction became more pronounced and rapid, resulting in an increased amount of TCh that consumed MnO<sub>2</sub> nanosheets. The alteration in the two-channel intensity ratio  $F_{468}/F_{558}$  tended to stabilise at higher AChE activity. The study also evaluated the linearity of the change in the two-channel intensity ratio  $F_{468}/F_{558}$  for various AChE activities while maintaining the same enzyme substrate concentration. The linear

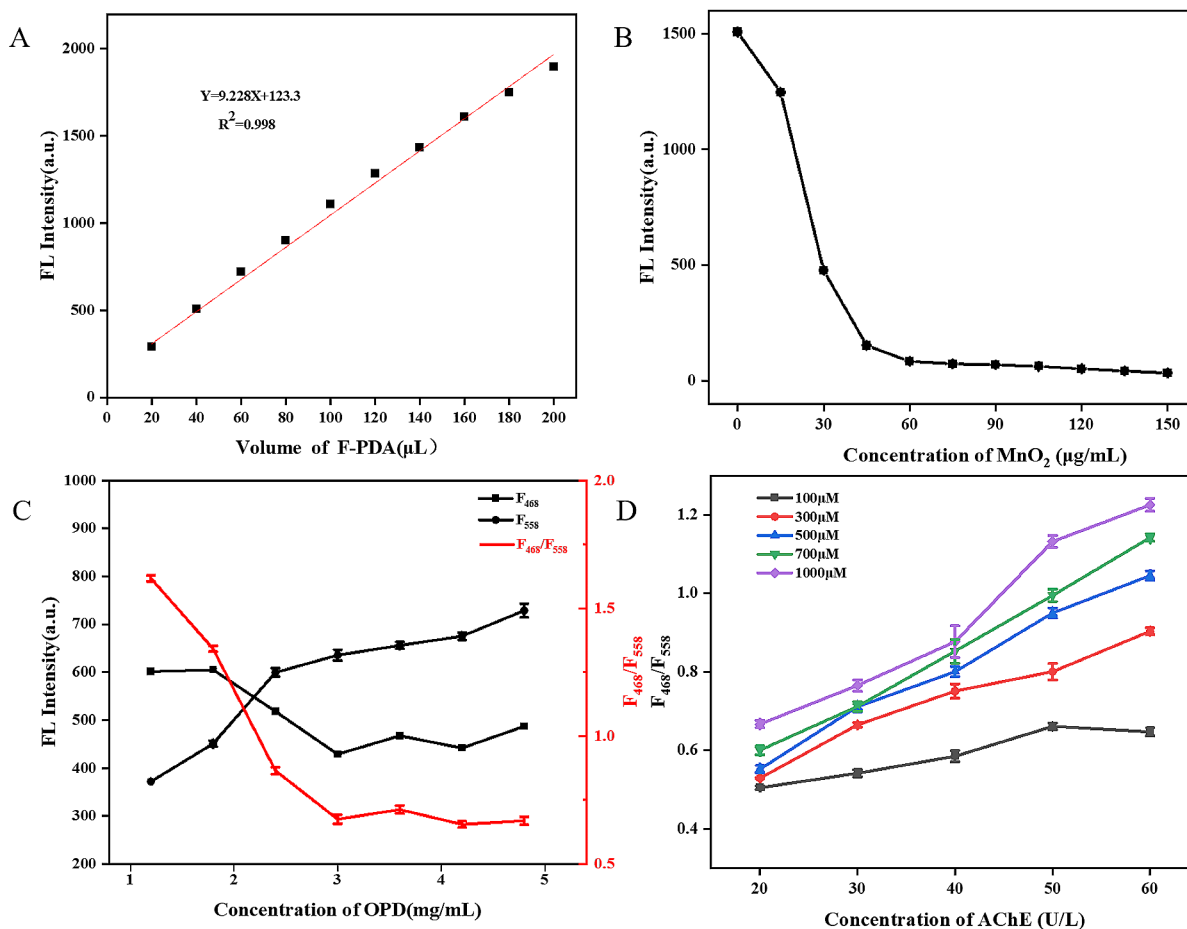


**Fig. 3** (A) Optimization of F-PDA volume. (B) The fluorescence intensity of F-PDA-MnO<sub>2</sub> with different concentration of MnO<sub>2</sub> nanosheet. (C) The fluorescence intensity of the system with different concentra-

tion of OPD. (D) The Fluorescence intensity of the system with various concentrations of enzyme substrate ATCh and AChE. regression values of the  $F_{468}/F_{558}$  ratio were  $R^2 = 0.9912$  and  $R^2 = 0.9977$  at enzyme substrate concentrations of 500 μM and 700 μM, respectively. Based on the detection range of AChE activity and the corresponding fluorescence intensity changes, the optimal concentration of ATCh was found to be 700 μM.

### Calibration Curve and Selectivity of AChE Activity

Under optimal conditions, the activity of AChE was analysed by the MnO<sub>2</sub>-F-PDA-OPD platform. As shown in the Fig. 4A, the increase of AChE concentration led to the decomposition of more MnO<sub>2</sub> nanosheets, which caused gradual enhancement on the fluorescence emission at 468 nm, and decrement on the fluorescence at 558 nm. In Fig. 4B, the fluorescence ratio at  $F_{468}/F_{558}$  served as the signal output for AChE detection, which exhibited two linear relationships within the concentration ranges of 0.05–1.0

and 1.0–48 U·L<sup>-1</sup>. The regression equations were derived to be  $Y = 0.087X + 1.015$  and  $Y = 0.00703X + 1.121$ , along with the corresponding regression coefficients of 0.9929 and 0.9917, respectively. In the equation, Y is the fluorescence intensity ratio  $F_{468}/F_{558}$  of the F-PDA-MnO<sub>2</sub>-OPD system at 468 nm and 558 nm, and X is the concentration of AChE. The limit of detection (LOD) for AChE was calculated to be 0.073 U·L<sup>-1</sup> ( $LOD = 3\sigma/S$ , where S is the slope of the first linear equation and  $\sigma$  is the standard deviation of 11 blank samples.)

The platforms MnO<sub>2</sub>-F-PDA and MnO<sub>2</sub>-OPD were also analysed to investigate the activity of AChE. As illustrated in Fig. S8 and Fig. S9, with increasing AChE concentration, more MnO<sub>2</sub> nanosheets were degraded, resulting in a gradual increase in fluorescence emission of F-PDA and a corresponding decrease in fluorescence emission of ox-OPD. Accordingly, the signal output for AChE detection was obtained using the fluorescence intensity value at  $F_{468}$ ,

and 1.0–48 U·L<sup>-1</sup>. The regression equations were derived to be  $Y = 0.087X + 1.015$  and  $Y = 0.00703X + 1.121$ , along with the corresponding regression coefficients of 0.9929 and 0.9917, respectively. In the equation, Y is the fluorescence intensity ratio  $F_{468}/F_{558}$  of the F-PDA-MnO<sub>2</sub>-OPD system at 468 nm and 558 nm, and X is the concentration of AChE. The limit of detection (LOD) for AChE was calculated to be 0.073 U·L<sup>-1</sup> ( $LOD = 3\sigma/S$ , where S is the slope of the first linear equation and  $\sigma$  is the standard deviation of 11 blank samples.)

The platforms MnO<sub>2</sub>-F-PDA and MnO<sub>2</sub>-OPD were also analysed to investigate the activity of AChE. As illustrated in Fig. S8 and Fig. S9, with increasing AChE concentration, more MnO<sub>2</sub> nanosheets were degraded, resulting in a gradual increase in fluorescence emission of F-PDA and a corresponding decrease in fluorescence emission of ox-OPD. Accordingly, the signal output for AChE detection was obtained using the fluorescence intensity value at  $F_{468}$ ,

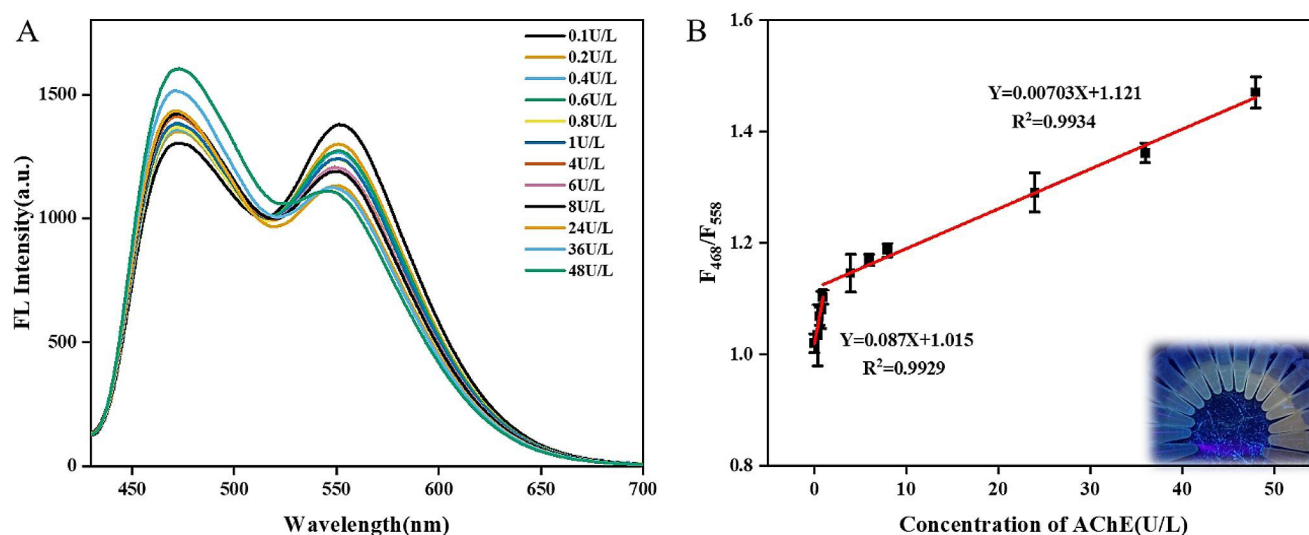


**Fig. 4** (A) Fluorescence spectra of the  $\text{MnO}_2$ -F-PDA-OPD system by incubation with various concentrations of AChE. (B) The corresponding calibration graphs for the  $\text{MnO}_2$ -F-PDA-OPD sensing system

**Table 1** Comparison of different detection methods for AChE activity

Methods	System	Linear range( $\text{U}\cdot\text{L}^{-1}$ )	Detection limit ( $\text{U}\cdot\text{L}^{-1}$ )	References
Electrochemistry	Screen-printed graphene electrodes	100–1500	100	[27]
Colorimetry	ATCh-TMB- $\text{H}_2\text{O}_2$	2–14.0	0.5	[28]
Colorimetry	AuNPs	0–5.0	0.46	[29]
Fluorometry (Non-ratiometric)	poly T-CuNPs	0.11–2.78	0.05	[30]
Fluorometry (Non-ratiometric)	Tetraphenylethylene functionalized with maleimide	0.3–3	0.089	[31]
Fluorometry (Non-ratiometric)	Gold-silver Nanocluster	0.4–25	0.15	[32]
Fluorometry (Ratiometric)	GQDs/ $\text{MnO}_2$ /OPD	0.1–2.0 2.0–4.5	0.09	[33]
Fluorometry (Ratiometric)	Fe-SAs/NC and PVP-CuNCs	2–70	0.56	[34]
Fluorometry (Ratiometric)	$\text{g-C}_3\text{N}_4$ / $\text{MnO}_2$	0.5–9	0.19	[25]
Fluorometry (Ratiometric)	$\text{MnO}_2$ -F-PDA/OPD	0.05–1.0 1.0–50	0.073	This work

which demonstrated two linear relationships in the concentration ranges of  $0.1 \sim 6.0$  and  $6.0 \sim 16 \text{ U}\cdot\text{L}^{-1}$  (Fig. S8). The regression equations for this study were  $Y = 0.3533X + 1.088$  and  $Y = 0.07487X + 2.583$ , with regression coefficients of 0.9907 and 0.9980, respectively. The detection limit was found to be  $0.044 \text{ U}\cdot\text{L}^{-1}$  ( $S/N=3$ ,  $n=11$ ). The fluorescence intensity value at  $F_{558}$  served as the signal output of the AChE assay, indicating a linear relationship that spanned the concentration range of  $6.0$  to  $60 \text{ U}\cdot\text{L}^{-1}$  (Fig. S9). The regression equation is  $Y = 0.00777X + 0.3004$  with a regression coefficient of 0.9903 and the limit of detection is  $0.69 \text{ U}\cdot\text{L}^{-1}$  ( $S/N=3$ ,  $n=11$ ). In the equation, Y represents the fluorescence intensity ratio  $(F-F_0)/F_0$  for the  $\text{MnO}_2$ -F-PDA and  $\text{MnO}_2$ -OPD system and X represents the concentration of AChE.

Compared with single channel fluorescence measurement, the  $\text{MnO}_2$ -F-PDA-OPD system biosensor has a dual detection function that reduces interference, while the change in fluorescence colour makes the results more intuitive. In addition, the sensor system has the ability to detect AChE activity over a wide range, making it suitable for a wider range of applications. The corresponding color change is further verified, which shows green to yellow trend as the AChE concentration increased from 0 to  $48 \text{ U}\cdot\text{L}^{-1}$ . The analytical performances of the present ratiometric fluorescence sensing system for the assay of AChE were compared with various protocols previously reported (Table 1). It is obvious that among the pile of approaches the present protocol provided favorable assay sensitivity and fulfil the requirements for the detection of both low and higher activity AChE.



## Specificity of the Sensing System

In order to evaluate the specificity of the ratiometric fluorescence probe for the assay of AChE, a number of disruptors (amino acids, proteins, enzymes, and other small molecules) were investigated under the optimal experimental conditions. These include amino acids (L-Serine), proteins (bovine serum albumin, enzymes (Amylase, lipase,  $\beta$ -Glucosidase, Cellulase) and other small molecules (glucose). Figure 5A illustrated that except for AChE, the above tested substances displayed virtually no obvious variation on the ratio fluorescence at  $F_{468}/F_{558}$  with respect to that of the control system at the same concentration or under the same activity condition, which was significantly different from the two-channel intensity ratio response induced by the target analyte. This indicated favorable selectivity of the F-PDA-MnO<sub>2</sub>-OPD ratiometric fluorescence probing system for the recognition of AChE.

## Screening of Inhibitor

Huperzine-A is an acetylcholinesterase inhibitor extracted from natural plants. To further evaluate the potential application of this method in the screening of AChE inhibitors, a typical inhibitor huperzine-A was used as the analytical model. By analyzing the inhibitory effect of huperzine-A at different concentrations on AChE, the half-maximal inhibitory concentration (IC<sub>50</sub>) of huperzine-A was obtained. Figure 5B displays the effect of huperzine-A with different concentrations on the fluorescence of the system. As the concentration of huperzine-A gradually increases from 0 to 100  $\mu\text{g}\cdot\text{mL}^{-1}$ , the fluorescence intensity at 468 nm gradually decreases and the fluorescence intensity at 558 nm gradually increases. This is because higher concentration of huperzine-A inhibits more AChE, resulting in the decrease of thiocholine and less MnO<sub>2</sub> nanosheets are decomposed. The inhibition rate can be determined by the equation  $\text{IE}(\%) = (F_0 - F_1) / (F_0 - F_1) \times 100\%$ , where  $F_1$  and  $F_0$  represented

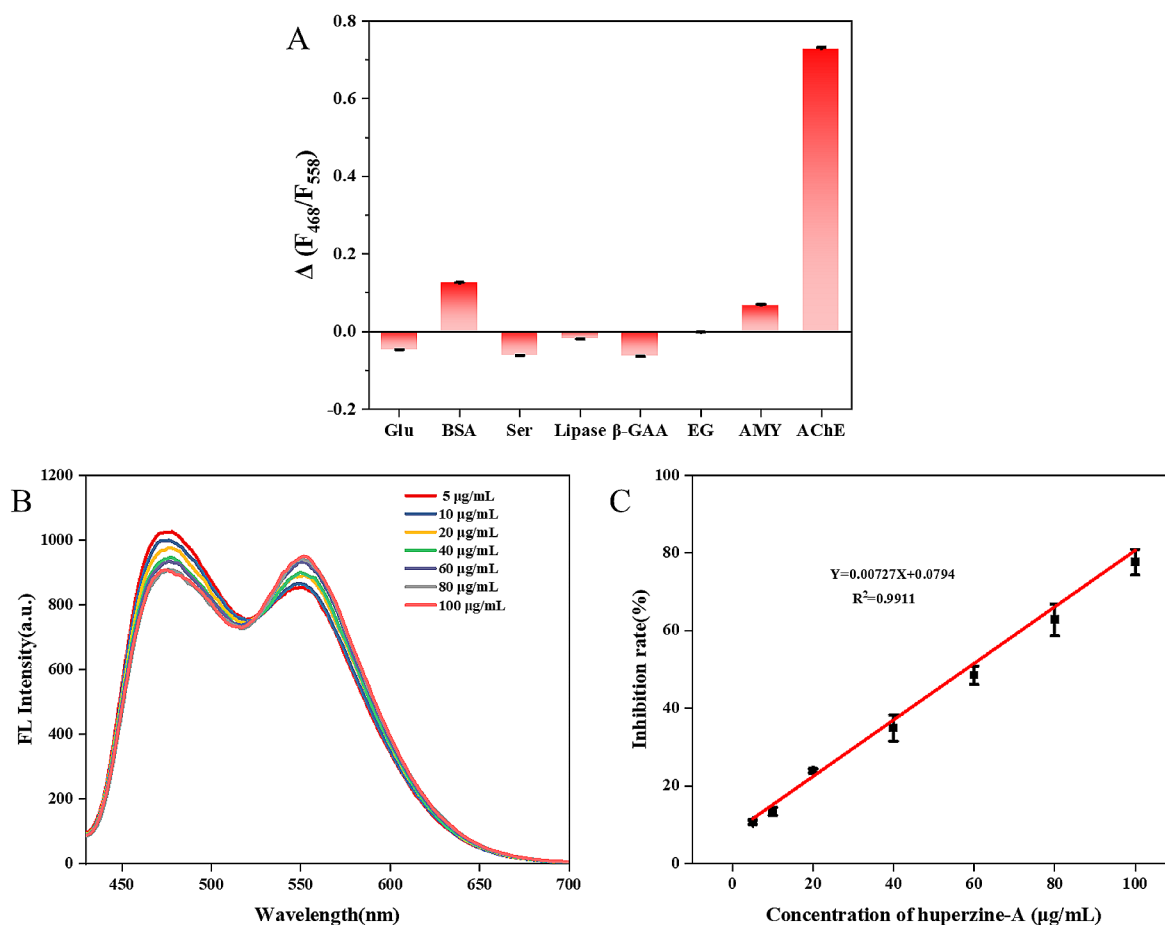


**Fig. 5** (A) Fluorescence ratio responses to various coexisting species. (B) Fluorescence spectra of the detection system with huperzine-A at different concentrations. (C) Relationship between the inhibition efficiency of AChE and the concentration of huperzine-A

the fluorescence ratio  $F_{468}/F_{558}$  in the absence and presence of inhibitor, respectively, while  $F_0$  represented the fluorescence ratio  $F_{468}/F_{558}$  in the absence of AChE and inhibitor [35].

As shown in Fig. 5C, the inhibitory efficiency of AChE increases with the gradual enhancement of inhibitor concentration. Generally, the change in fluorescence intensities of the proposed system further confirmed the correlation between the inhibition efficiencies and huperzine-A concentrations. The inhibition rate served as the signal output of the AChE assay, indicating a linear relationship that spanned the concentration range of 5 to 100  $\mu\text{g}\cdot\text{mL}^{-1}$ . By fitting the relationship between the inhibition efficiency and the concentration of huperzine-A, the regression equations for this study were  $Y=0.00727X+0.0794$  with regression coefficients of 0.9911. Therefore, the inhibition ability of vanillic acid, quinine, geniposide, and berberine on AChE activity were separately investigated based on the designed method. In conclusion, the method showed good application potential to screen inhibitors from natural products.

## Conclusion

In conclusion, we developed and integrated simple fluorescent indicators to establish a  $\text{MnO}_2$ -based ratiometric fluorescent probe with the help of the excellent catalytic properties of  $\text{MnO}_2$  nanosheets to detect the activity of AChE. The ratiometric fluorescence sensing system was demonstrated by the assay of AChE activity. Compared with the conventional single-channel fluorescence sensing detectors F-PDA- $\text{MnO}_2$  and OPD- $\text{MnO}_2$ , the ratiometric fluorescence sensing system proposed in this study has a wider quantitative range and a more obvious colour change for the detection of AChE. Moreover, the method has achieved the quantitative assay of AChE activity with a wide linear range and a low LOD of 0.073  $\text{U}\cdot\text{L}^{-1}$ . Huperzine-A were chosen as an example to demonstrate the promising application in inhibitor screening. The above results indicated that the method had certain practicability and application potential in the clinical diagnosis of AChE and the screening of inhibitors.

**Supplementary Information** The online version contains supplementary material available at <https://doi.org/10.1007/s10895-024-03703-y>.

**Author Contributions** FZ (First Author): Conceptualization, Methodology, Software, Investigation, Formal Analysis, Writing - Original Draft, Writing - Review & Editing; HG (Corresponding Author): Conceptualization, Funding Acquisition, Resources, Supervision, Writing - Review & Editing; WY: Data Curation, Writing - Original Draft; LG: Resources, Supervision; JL: Visualization, Investigation; HC: Software, Validation.

**Funding** The authors declare that no funds, grants, or other support were received during the preparation of this manuscript.

**Data Availability** No datasets were generated or analysed during the current study.

## Declarations

**Competing Interests** The authors declare no competing interests.

## References

1. Yan X, Song Y, Wu X, Zhu C, Su X, Du D, Lin Y (2017) *Nanoscale* 9:2317–2323. <https://doi.org/10.1039/C6NR08473G>
2. Liu D-M, Xu B, Dong C (2021) *TrAC Trends Anal Chem* 142:116320. <https://doi.org/10.1016/j.trac.2021.116320>
3. Zhang X-P, Xu W, Wang J-H, Shu Y (2022) *Analyst* 147:4008–4013. <https://doi.org/10.1039/D2AN01180H>
4. Pourshojaei Y, Abiri A, Eskandari K, Haghighijoo Z, Edraki N, Asadipour A (2019) *Sci Rep* 9:19855. <https://doi.org/10.1038/s41598-019-56463-2>
5. Liu J, Ma R, Ha W, Zhang H-X, Shi Y-P (2023) *Talanta* 253. <https://doi.org/10.1016/j.talanta.2022.124025>
6. Ye M, Lin B, Yu Y, Li H, Wang Y, Zhang L, Cao Y, Guo M (2020) *Microchim Acta* 187:511. <https://doi.org/10.1007/s00604-020-04522-1>
7. Wang Y, Zhao Q, Xue Y, Wu D, Zhang B, Sun J, Yang X (2023) *Sens Actuators B* 396:134565. <https://doi.org/10.1016/j.snb.2023.134565>
8. Oe M, Miki K, Masuda A, Nogita K, Ohe K (2022) *Chem Commun* 58:1510–1513. <https://doi.org/10.1039/d1cc05132f>
9. Ouyang H, Lu Q, Wang W, Song Y, Tu X, Zhu C, Smith JN, Du D, Fu Z, Lin Y (2018) *Anal Chem* 90:5147–5152. <https://doi.org/10.1021/acs.analchem.7b05247>
10. Chen Q, Yang L-P, Li D-H, Zhai J, Jiang W, Xie X (2021) *Sens Actuators B* 326:128836. <https://doi.org/10.1016/j.snb.2020.128836>
11. Xing L, Ma P, Chen F (2024) *Spectrochim Acta Part A* 310:123954. <https://doi.org/10.1016/j.saa.2024.123954>
12. Yang M, Zhou H, Zhang Y, Hu Z, Niu N, Yu C (2018) *Microchim Acta* 185:132. <https://doi.org/10.1007/s00604-018-2678-9>
13. Han Y, Ye Z, Wang F, Chen T, Wei L, Chen L, Xiao L (2019) *Nanoscale* 11:14793–14801. <https://doi.org/10.1039/C9NR01817D>
14. Xiao SJ, Chu ZJ, Zhao XJ, Zhang ZB, Liu YH (2017) *Microchim Acta* 184:4853–4860. <https://doi.org/10.1007/s00604-017-2519-2>
15. Halawa MI, Wu F, Zafar MN, Mostafa IM, Abdussalam A, Han S, Xu G (2020) *J Mater Chem B* 8:3542–3549. <https://doi.org/10.1039/C9TB02158B>
16. Fan D, Shang C, Gu W, Wang E, Dong S (2017) *ACS Appl Mater Interfaces* 9:25870–25877. <https://doi.org/10.1021/acsami.7b07369>
17. Zhang Z, Feng J, Huang P, Li S, Wu F-Y (2019) *Sens Actuators B* 298. <https://doi.org/10.1016/j.snb.2019.126891>
18. Niu C, Liu Q, Shang Z, Zhao L, Ouyang J (2015) *Nanoscale* 7:8457–8465. <https://doi.org/10.1039/c5nr00554j>
19. Huang Z-M, Cai Q-Y, Ding D-C, Ge J, Hu Y-L, Yang J, Zhang L, Li Z-H (2017) *Sens Actuators B* 242:355–361. <https://doi.org/10.1016/j.snb.2016.11.066>
20. Xiao T, Sun J, Zhao J, Wang S, Liu G, Yang X (2018) *ACS Appl Mater Interfaces* 10:6560–6569. <https://doi.org/10.1021/acsami.7b18816>

21. Qu F, Yan H, Li K, You J, Han W (2020) *J Mater Sci* 55:10022–10034. <https://doi.org/10.1007/s10853-020-04754-9>
22. Zhou Q, Zhou T, Tu Y, Yan J (2023) *Chem Pap* 77:3671–3678. <https://doi.org/10.1007/s11696-023-02729-z>
23. Luo L, Fei J, Duan X, Qi Y, Li M, Li H, Huang J (2019) *Tribol Int* 134:145–153. <https://doi.org/10.1016/j.triboint.2019.01.044>
24. Liu Y, Ai K, Lu L (2014) *Chem Rev* 114:5057–5115. <https://doi.org/10.1021/cr400407a>
25. Zhang Y, Wu Y, Liu L, Wang W, Zhang W, Song D, Wang X, Su R (2021) *Sens Actuators B* 346:130531. <https://doi.org/10.1016/j.snb.2021.130531>
26. Zhang J, Yang H, Pan S, Liu H, Hu X (2021) *Spectrochim Acta Part A* 244. <https://doi.org/10.1016/j.saa.2020.118831>
27. Panraksa Y, Siangproh W, Khampieng T, Chailapakul O, Api-lux A (2018) *Talanta* 178:1017–1023. <https://doi.org/10.1016/j.talanta.2017.08.096>
28. Han T, Wang G (2019) *J Mater Chem B* 7:2613–2618. <https://doi.org/10.1039/c8tb02616e>
29. Lv J, He B, Wang N, Li M, Lin Y (2018) *RSC Adv* 8:32893–32898. <https://doi.org/10.1039/c8ra06165c>
30. Ni P, Sun Y, Jiang S, Lu W, Wang Y, Li Z, Li Z (2017) *Sens Actuators B* 240:651–656. <https://doi.org/10.1016/j.snb.2016.08.096>
31. Chang J, Li H, Hou T, Li F (2016) *Biosens Bioelectron* 86:971–977. <https://doi.org/10.1016/j.bios.2016.07.022>
32. Liu R, Wu Z, Yang Y, Liao S, Yu R (2018) *Mater Res Express* 5:065027. <https://doi.org/10.1088/2053-1591/aac867>
33. Ye M, Lin B, Yu Y, Li H, Wang Y, Zhang L, Cao Y, Guo M (2020) *Mikrochim Acta* 187:511. <https://doi.org/10.1007/s00604-020-04522-1>
34. Wang M, Liu L, Xie X, Zhou X, Lin Z, Su X (2020) *Sens Actuators B* 313:128023. <https://doi.org/10.1016/j.snb.2020.128023>
35. Wang Y, Xue Y, Zhao Q, Wang S, Sun J, Yang X (2022) *Anal Chem* 94:16345–16352. <https://doi.org/10.1021/acs.analchem.2c03290>

**Publisher's Note** Springer Nature remains neutral with regard to jurisdictional claims in published maps and institutional affiliations.

Springer Nature or its licensor (e.g. a society or other partner) holds exclusive rights to this article under a publishing agreement with the author(s) or other rightsholder(s); author self-archiving of the accepted manuscript version of this article is solely governed by the terms of such publishing agreement and applicable law.